Journal of Molecular Catalysis A: Chemical 342–343 (2011) 83–90

Contents lists available at ScienceDirect

Journal of Molecular Catalysis A: Chemical

journal homepage: www.elsevier.com/locate/molcata

Zn,Al hydrotalcites calcined at different temperatures: Preparation, characterization and photocatalytic activity in gas–solid regime

D. Carriazo[a,1], M. del Arco[a], E. García-López[b,*], G. Marcì[b], C. Martín[a], L. Palmisano[b], V. Rives[a]

[a] GIR-QUESCAT, Departamento de Química Inorgánica, Universidad de Salamanca, 37008 Salamanca, Spain
[b] "Schiavello-Grillone" Photocatalysis Group, Dipartimento di Ingegneria Elettrica, Elettronica e delle Telecomunicazioni, di Tecnologie Chimiche, Automatica e Modelli Matematici (DIEETCAM), Università di Palermo, Viale delle Scienze, 90128 Palermo, Italy

ARTICLE INFO

Article history:
Received 7 February 2011
Received in revised form 13 April 2011
Accepted 21 April 2011
Available online 30 April 2011

Keywords:
Layered double hydroxides
Photocatalysis
$ZnAl_2O_4$
ZnO

ABSTRACT

Layered double hydroxides (LDH) containing zinc and aluminium within the brucite-like layers and carbonate as the interlayer anion have been used as precursors for the preparation of mixed metal oxides by calcination. Zinc oxide and the $ZnAl_2O_4$ spinel were formed with different degree of crystallinity depending of two parameters, i.e., the Zn^{2+}/Al^{3+} molar ratio and the calcination temperature (500–800 °C) of the LDH precursor. A pure spinel phase was obtained to remove ZnO upon a basic post-treatment in NaOH solution of the samples calcined at 800 °C. All the samples were tested for the photodegradation of 2-propanol in gas–solid regime. All the samples resulted active as heterogeneous photocatalysts. The photocatalytic activity increased by increasing the Zn^{2+}/Al^{3+} molar ratio and the calcination temperature of the solids.

1. Introduction

There is an increasing demand for catalysts to eliminate the pollution associated to toxic compounds. Semiconductors such as TiO_2 [1,2], ZnO [3,4], SnO_2 or CdS [5] have been used in photocatalytic degradation of organic pollutants in liquid–solid [6] and in gas–solid regimes [7]. In addition to these oxides, it is worth studying the photoactivity of metal spinels, such as $ZnAl_2O_4$, which band gap, 3.8 eV [8], makes it suitable for photocatalytic processes [9]. The classic route for preparation of semiconductor metal oxides photocatalysts, commonly obtained by calcination of salts, leads to solids with low specific surface area which is a disadvantage in heterogeneous catalysis. To avoid this problem various preparation methods such as sol–gel processes have been proposed [10]. The sol–gel methodology allows to obtain materials with high specific surface area, but the nature of the precursors, generally metal alkoxides, makes it very expensive. An alternative preparation method is the calcination of layered double hydroxides (LDHs), also known as hydrotalcite-like compounds or anionic clays [11–14]. These materials are layered solids with positively charged sheets, due to isomorphic substitution of divalent cations by trivalent ones in brucite layers, and charge-balancing anions in the interlayer space. These solids can be described by the general formula $[M^{3+}_xM^{2+}_{1-x}(OH)_2]^{x+}\,[A^{n-}]_{x/n}\,mH_2O$ where M^{2+} and M^{3+} are the divalent and the trivalent cation, respectively, and A^{n-} the exchangeable anion in the interlayer, where water molecules are also found. LDHs easy preparation, low cost and physico-chemical properties have allowed many applications for these materials as catalysts, catalyst supports and precursors, adsorbents, drug matrices, etc. [11–13]. The LDH compounds as prepared or calcined by a controlled decomposition are often used as catalysts or catalyst precursors. LDHs calcination have resulted to be an excellent methodology to prepare mixed oxides with better catalytic performance than conventional preparations, such as ceramic or wet chemical routes. For instance, Qi et al. have recently conducted studies on a mixed oxide catalyst prepared by calcination of LDHs which exhibited a comparable activity, but better stability compared with a commercial Cu-based catalyst [15]. Also Li et al. have reported that pure spinel ferrites can be obtained by calcination of tailored hydrotalcite-like layered double hydroxides [16]. These authors report that the main advantage of this preparation methodology is that the uniform distribution of metal cations in the LDH precursors drives to the formation of spinel ferrites in shorter time and requiring a much lower temperature.

In this work, Zn,Al hydrotalcites with different Zn^{2+}/Al^{3+} molar ratios and carbonate as the interlayer anion have been prepared. After their calcination at different temperatures (500–800 °C) the photocatalytic activity of the materials was tested for 2-propanol oxidation in gas–solid regime. Photocatalytic oxidation of 2-propanol by using various types of solids is a widely studied

* Corresponding author. Tel.: +39 091 23863784; fax: +39 091 7025020.
E-mail address: elisaisabel.garcialopez@unipa.it (E. García-López).
[1] Current address: Instituto de Ciencia de Materiales de Madrid, CSIC, Cantoblanco, 28049 Madrid, Spain.

1381-1169/$ – see front matter © 2011 Elsevier B.V. All rights reserved.
doi:10.1016/j.molcata.2011.04.015

reaction and different degradation pathways are reported depending upon the physico-chemical features of the solid [17]. Moreover, pure $ZnAl_2O_4$ spinel was obtained by selective leaching of ZnO from the hydrotalcites calcined at high temperature and their photocatalytic activity was also tested.

2. Experimental

2.1. Samples preparation

2.1.1. Synthesis of Zn/Al hydrotalcite precursors and oxides

Zn/Al hydrotalcite samples with carbonate in the interlayer (denoted hereafter as Zn/Al-CO_3 LDHs) have been prepared by the standard co-precipitation method from metal salts [14]. Zn and Al nitrates, in adequate quantities to get a molar Zn/Al ratio of 2 or 3, were added to a basic solution containing NaOH (2 M) and Na_2CO_3 (1 M), at pH 9 and 40 °C. The suspension, kept under constant magnetic stirring during the addition of the salts, was further stirred for 24 h at 70 °C. The resulting filtered powder was finally washed, centrifuged and dried in air. The obtained samples were named as Zn/Al-2 and Zn/Al-3, depending on the nominal Zn/Al molar ratio. They were calcined at 500, 600, 700 or 800 °C for 2 h, leading to the final solids which are named as the parent sample, followed by the calcination temperature in Celsius.

2.1.2. Synthesis of $ZnAl_2O_4$ spinels

Since calcination of hydrotalcites usually leads to formation of a mixture of the spinel and the oxide of the divalent cation, a pure spinel was obtained by selective leaching of ZnO from samples Zn/Al-3-700 and Zn/Al-3-800. A portion of 2 g of the Zn/Al-3-700 or Zn/Al-3-800 solid was added to 50 ml of NaOH 10 M and kept for 48 h at 60 °C under moderate agitation. The resulting suspension was centrifuged and washed several times until complete elimination of sodium and then dried at 80 °C overnight. The samples obtained were labelled as S-700 and S-800.

2.2. Characterization of the solids

Chemical analyses for Zn and Al were carried out in Servicio General de Análisis Químico Aplicado (Universty of Salamanca, Spain) in a model ULTIMA-2 ICP-OES spectrophotometer from Jovin Yvon, after dissolving the samples in nitric acid. Carbon was analyzed in an Elemental Analyzer from Leco, model CHNS 932. The powder X-ray diffraction (PXRD) patterns were collected on a Siemens D-500 diffractometer using Cu Kα radiation (λ 1.54050 Å) and quartz as an external standard. The textural properties were studied from the N_2 adsorption–desorption isotherms, recorded at −196 °C in a Gemini instrument from Micromeritics. The samples were previously outgassed at 120 °C for 2 h. Scanning electron microscopy (SEM) was performed using a FEI QUANTA 200-F ESEM microscope, operating at 20 kV on specimens upon which a thin layer of gold had been evaporated. The diffuse reflectance spectra (DRS) were obtained in air at room temperature in the wavelength range 800–250 nm using a Shimadzu UV-2401 PC spectrophotometer, with $BaSO_4$ as the reference material.

2.3. Photoreactivity experiments

The photoreactor operating in the gas–solid regime was a cylindrical shaped batch type Pyrex fixed bed photoreactor (V = 150 ml, Φ = 93 mm, height = 22 mm). The photocatalyst (0.1 g) was simply dispersed as a thin layer inside the photoreactor and the corresponding fixed bed height was ca. 1 mm. In this tightly closed reactor, after purging with pure O_2 during 30 min, 10 μL of liquid 2-propanol was injected and quickly vaporized with an infrared gun. The initial concentration of 2-propanol was 8.7×10^{-4} M.

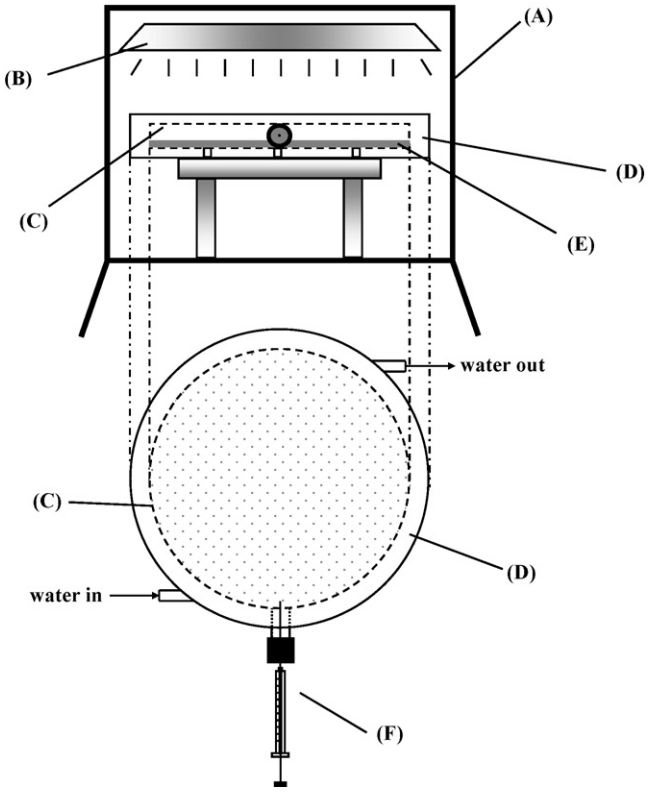

Scheme 1. Set up of the photoreactive system: (A) Solarbox; (B) lamp; (C) photoreactor; (D) water cooling jacket; (E) photocatalyst; and (F) gas-tight syringe.

The reactor, provided with a water cooling jacket, was horizontally positioned and illuminated from the top inside a SOLARBOX apparatus (CO.FO.ME.GRA.) equipped with a solar simulating lamp (1500 W high pressure Xe lamp). The set-up of the photoreactivity system is shown in Scheme 1.

Irradiation started only after the achievement of steady state conditions, i.e., after maintaining the system under dark conditions at room temperature to obtain the adsorption equilibrium of the substrate onto the catalyst surface. The irradiance reaching the photoreactor was measured by using a UVX Digital radiometer and it was equal to 1.0 mW cm^{-2} at a wavelength of 365 nm. The runs lasted ca. 5 h and the reacting fluid was analyzed by withdrawing gas samples from the photoreactor by means of a gas-tight syringe. The concentrations of the substrate and of the intermediates were measured by a GC-17A Shimadzu gas chromatograph equipped with a HP-1 column and a FID, whereas carbon dioxide was analyzed by a 60/80 Carboxen 1000 column in an HP6890 gas chromatograph equipped with a TCD.

3. Results and discussion

3.1. Bulk and textural samples characterization

Fig. 1 reports the PXRD patterns of the original hydrotalcite samples and of the oxides obtained after their calcination. The diffractograms of the uncalcined Zn/Al-2 and Zn/Al-3 samples are characteristic of well crystallized solids with the hydrotalcite-like structure. The only appreciable difference between them is the relative intensity of the diffraction lines, which appears sharper and more intense for Zn/Al-2 sample, indicating a higher degree of crystallinity in this solid [18]. The diffraction patterns of both materials show the peaks corresponding to the crystallographic planes (0 0 l) in a relatively symmetrical sequence indicating a high level of order in the stacks. The basal spacing values corresponding to diffraction

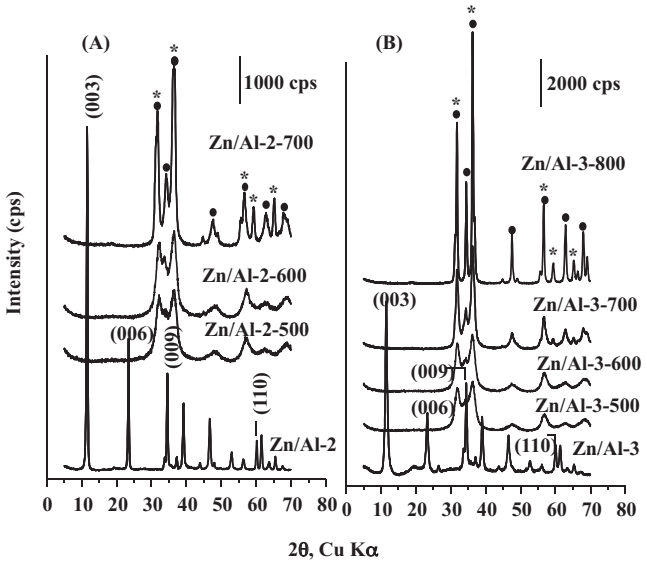

Fig. 1. PXRD diffractograms of Zn/Al-2 (A) and Zn/Al-3 (B) series. (●) ZnO zincite (*) $ZnAl_2O_4$. Crystallographic parameters of the Zn/Al-2 and Zn/Al-3: $a = 3.02 \pm 0.01$ Å and $c = 23.7 \pm 0.1$ Å.

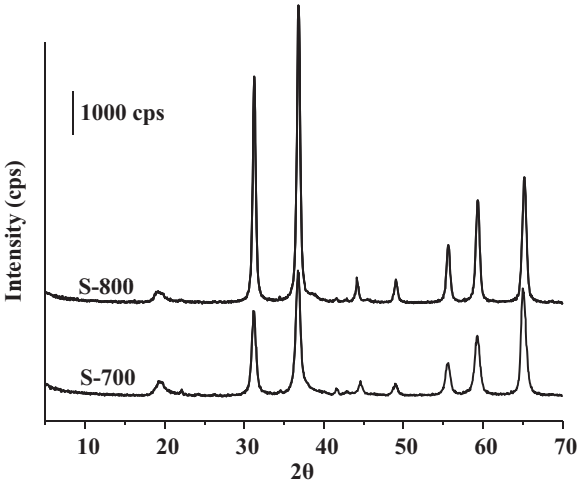

Fig. 2. PXRD diffractograms for (a) S-700 and (b) S-800.

by planes (0 0 3) and (0 0 6) and the crystallographic parameters ***a*** and ***c***, calculated from the positions of the diffraction lines corresponding to (1 1 0) and (0 0 3) planes, respectively [19], are in agreement with those calculated by other authors for similar samples [9,20,21]. Both diffraction patterns also show very low intense lines that can be tentatively ascribed to the presence of a crystalline ZnO phase dispersed over the brucite-like layers.

Calcination of the samples at 500 °C leads to the collapse of the lamellar structure and new diffraction lines ascribed to different metal oxides, ZnO and the $ZnAl_2O_4$ spinel, appear (see Fig. 1). These diffraction maxima are much weaker than those of the previous hydrotalcite-like phase, indicating the lower crystallinity of these phases. Patzkó et al. [21] previously reported that calcination at 500 °C is not enough to induce the formation of aluminium oxide crystals and they suggested that only ZnO crystallizes at this temperature, whereas Al is present as AlO(OH). On the contrary Zou et al. [9] claimed that crystallization of both ZnO (zincite) and $ZnAl_2O_4$ spinel occurred at 500 °C, and they reported that the use of hydrotalcite as the starting material for the formation of the spinel required short time and low temperature. In another study, Zhao et al. [22] considered that Al^{3+} cations are homogeneously dispersed in a mostly amorphous phase and they are leached at 500 °C from ZnO, giving rise to formation of spinel phase. It can be also observed in Fig. 1 that calcination at higher temperatures (>500 °C) resulted in an increase in the crystallinity of both ZnO and $ZnAl_2O_4$, as suggested by the higher intensity and sharpness of the maxima due to both phases.

Zn/Al-3-700 and Zn/Al-3-800 samples were treated with a NaOH solution at 60 °C in order to selectively remove the ZnO phase by dissolution. Fig. 2 reports the PXRD of the resulting samples (S-700 and S-800) where only peaks due to the $ZnAl_2O_4$ spinel can be observed. These peaks are particularly sharp for sample S-800.

Chemical analysis data (atomic absorption) of the samples indicated that the amounts of Zn and Al for the Zn/Al-2 (36.1% Zn, 7.5% Al) and Zn/Al-3 (48.9% Zn, 7.3% Al) samples are in acceptable agreement with the nominal Zn/Al molar ratio in the pristine solution during preparation of the hydrotalcites, which evidenced that the co-precipitation was nearly complete. The results, by taking into account also carbon analyses, allowed to calculate the following formulae: $[Zn_{0.66}Al_{0.33}(OH)_2](CO_3)_{0.17}\cdot nH_2O$ and $[Zn_{0.73}Al_{0.27}(OH)_2](CO_3)_{0.14}\cdot nH_2O$, for the solids Zn/Al-2 and Zn/Al-3, respectively.

As expected, the metal molar ratios measured, reported in Table 1, did not change significantly after the thermal treatments at different temperatures. The decrease of the Zn percentage in the samples after the treatment with NaOH confirmed dissolution of the ZnO phase. This was more evident for sample S-800 in which the measured Zn/Al molar ratio was close to 0.5, which corresponds to the theoretical ratio in a pure $ZnAl_2O_4$ spinel phase. Moreover, these measurements indicate also that ZnO is not completely leached in sample S-700, because the Zn/Al molar ratio corresponds to 1.42.

To study the textural properties of all of the samples, the adsorption–desorption isotherms of N_2 at −196 °C have been recorded. Fig. 3 shows the isotherms of some selected samples and Table 1 includes the values of the BET specific surface areas (SSA).

Calcination of samples at 500 °C led to an increase in the SSA, due to the destruction of the lamellar structure giving rise to the formation of low crystalline ZnO and $ZnAl_2O_4$ phases The crystallinity increased by increasing the calcination temperature and, therefore, the SSA values significantly decreased, as reported in Table 1. Calcination at 800 °C gave rise to sintering of the oxides and consequently to a strong decrease of their specific surface areas. Treatment with NaOH solution, for ZnO removal, led to an increase of their specific surface areas. Sample S-800 exhibited a specific surface area three times higher than that of the untreated sample and a pore volume ten times larger (0.02 $cm^3\ g^{-1}$ for the calcined sam-

Table 1
Molar ratio Zn/Al in the samples, band gap of the powders, specific surface areas (SSA) and amount of CO_2 evolved per unit of surface area after 5 h of photocatalytic reaction.

Sample	Zn/Al molar ratio	*E* gap [eV]	SSA [$m^2\ g^{-1}$]	CO_2 [mol/m^2]
Zn/Al-2	1.99	–	20	
Zn/Al-3	2.77	–	53	
Zn/Al-2-500	2.01	n.m.	64	Absent
Zn/Al-2-600	1.99	3.65	45	Absent
Zn/Al-2-700	2.10	3.30	25	1.9×10^{-6}
Zn/Al-3-500	2.88	3.32	84	1.6×10^{-6}
Zn/Al-3-600	2.83	3.41	72	3.2×10^{-6}
Zn/Al-3-700	3.02	3.33	48	5.6×10^{-6}
Zn/Al-3-800	3.20	3.30	18	1.7×10^{-5}
S-700	1.42	3.20	57	2.6×10^{-6}
S-800	0.50	–	50	1.4×10^{-6}
ZnO Aldrich	–	3.20	19	1.3×10^{-5}

(n.m. = not measured).

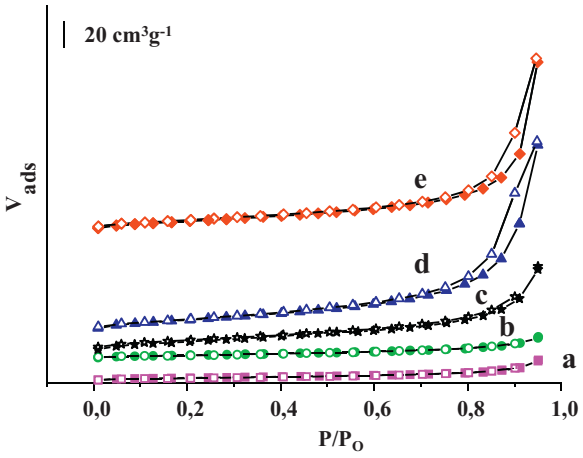

Fig. 3. Nitrogen adsorption–desorption isotherms (filled symbols and open symbols, respectively) at −196 °C for (a) Zn/Al-2; (b) Zn/Al-3-800; (c) Zn/Al-3-500; (d) S-700 and (e) S-800.

ple and 0.2 $cm^3\ g^{-1}$ for sample S-800). The adsorption–desorption isotherms are characteristic of nonrestricted multilayer adsorption on nonporous samples and they correspond to the type II according to the IUPAC classification [23]. Samples S-700 and S-800 obtained after the ZnO leaching are an exception to this behaviour, as their isotherms are characteristic of mesoporous solids (type IV of the IUPAC classification). The latter also exhibits a H3 hysteresis loop, indicating some asymmetry of the pores.

From SEM observations (see Figs. 4 and 5), it can be concluded that the platelet-like morphology of the starting hydrotalcite samples was maintained for both Zn/Al-2 and Zn/Al-3 sets of samples, without any appreciable difference up to a temperature of 700 °C. Calcination at 800 °C produced the collapse of this morphology and larger particles with rounded edges are observed. The morphology of samples S-700 and S-800 is completely different from that of the samples not treated with NaOH. Indeed, they consist of aggregates of particles with sizes of ca. 30 nm and 90 nm for samples S-700 and S-800, respectively. The higher increase of SSA (from 18 to 50 $m^2\ g^{-1}$) for Zn/Al-3-800 and S-800 in respect to Zn/Al-3-700 and S-700 (from 48 to 57 $m^2\ g^{-1}$) (see Table 1), can be attributed to the complete removal of ZnO in sample S-800 (consisting of $ZnAl_2O_4$) and to the residual presence of ZnO in sample S-700.

Fig. 6 shows the diffuse reflectance spectra of the calcined Zn/Al-2 and -3 samples. All calcined Zn/Al-2 and -3 samples showed the typical broad absorption band that can be ascribed to the charge transfer process from O^{2-} to Zn^{2+} responsible for the ZnO band-gap. The only exception is sample Zn/Al-2-500, (Fig. 6(a)) whose spectrum shows a step. When the calcination temperature increased (see sample Zn/Al-2-600, Fig. 6(b)), this step disappeared. A further increase of the calcination temperature gave rise to a shift to lower energies; indeed, absorption of sample Zn/Al-2-600 starts at ca. 370 nm (Fig. 6(b)), whereas the absorption of sample Zn/Al-2-700 starts at ca. 425 nm (Fig. 6(c)). As far as the calcined Zn/Al-3 sample concerns, the spectrum for sample Zn/Al-3-500 (Fig. 6(d)) shows only a broad absorption band that is shifted to higher energies for the Zn/Al-3-600 sample (Fig. 6(e)), but again, as in the case of the Zn/Al-2 samples, it is shifted to lower energies for samples calcined at a higher temperature (Zn/Al-3-700, Fig. 6(f)).

Since the band gaps for $ZnAl_2O_4$ and ZnO are reported to be 3.8 and 3.2 eV, respectively [8], the shift to higher energies in the absorption edge could be due to a more important presence of the spinel structure at 600 °C with respect to 500 °C, in agreement with the PXRD diffractograms. Moreover, when the calcination temperature increased from 600 up to 800 °C the crystallinity of the ZnO particles increased (see Fig. 1) and consequently the absorption by this material is recorded at lower energies.

The presence of the step in the spectrum of the Zn/Al-2-500 sample, which is absent in the spectrum of sample Zn/Al-3-500, can be due to the fact that the spectrum of sample Zn/Al-2-500

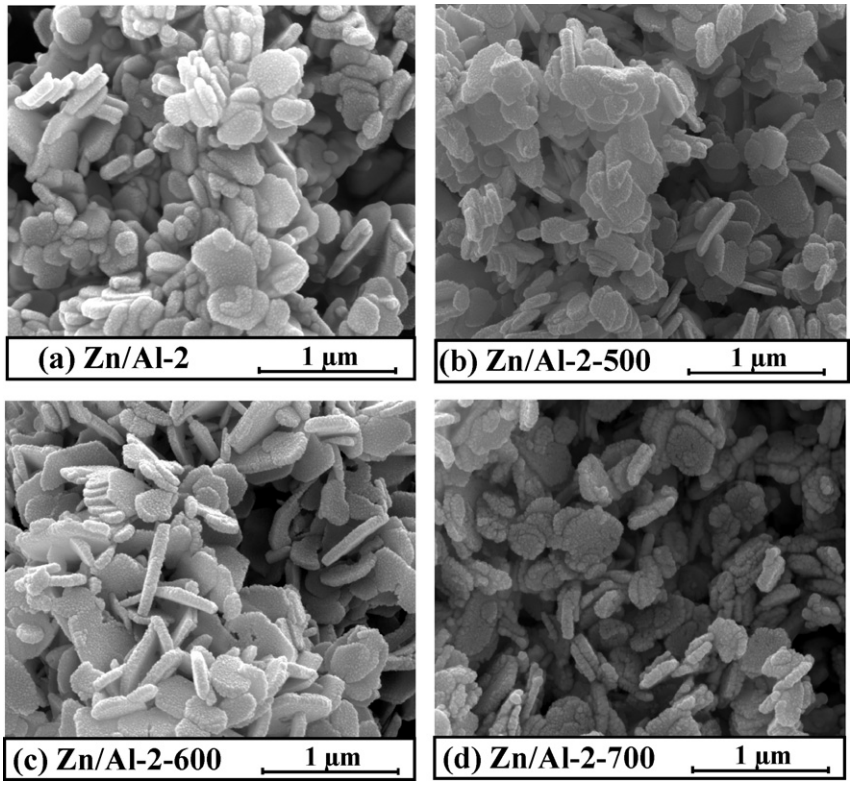

Fig. 4. SEM micrographs for (a) Zn/Al-2; (b) Zn/Al-2-500; (c) Zn/Al-2-600 and (d) Zn/Al-2-700.

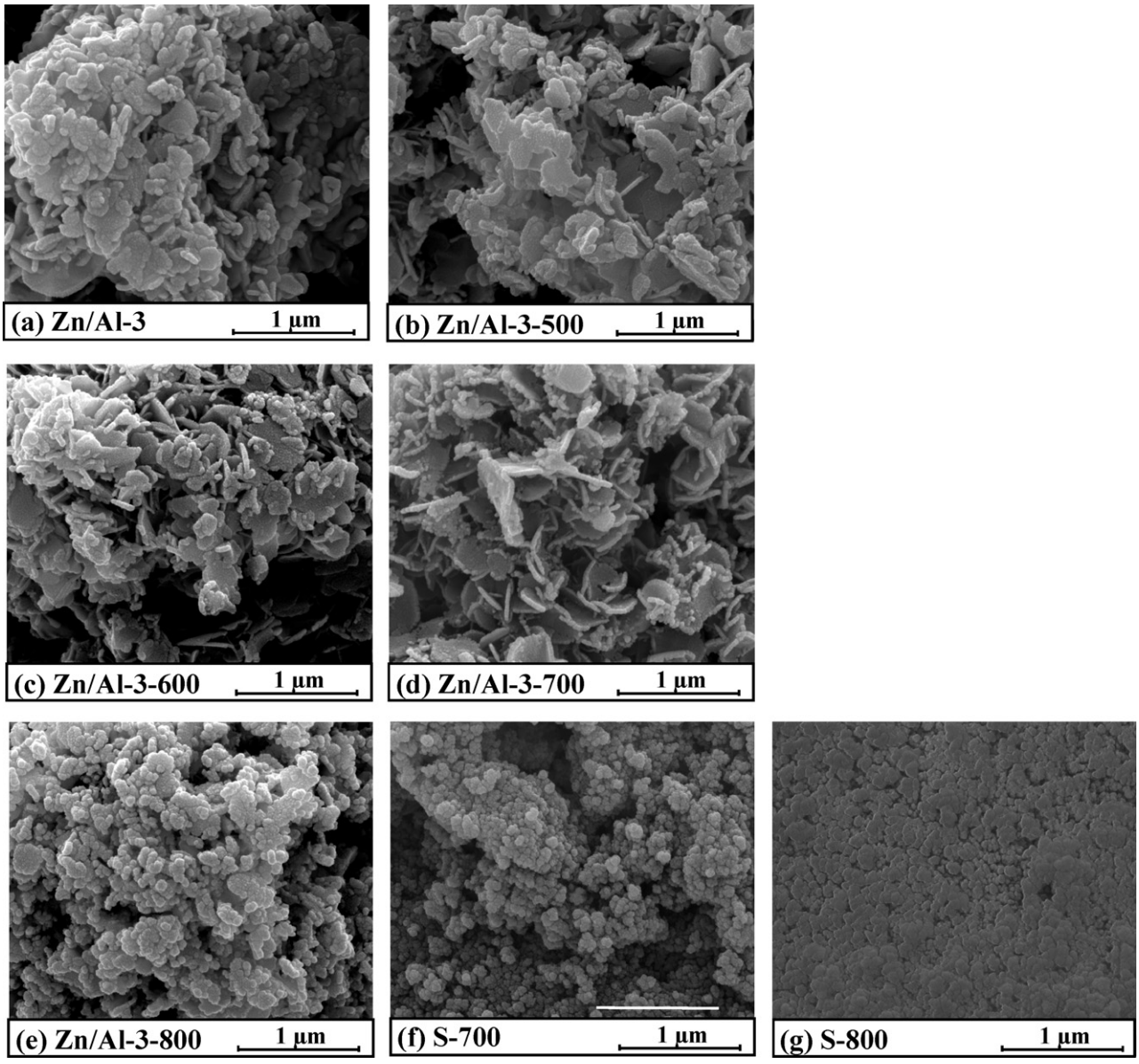

Fig. 5. SEM micrographs for (a) Zn/Al-3; (b) Zn/Al-3-500; (c) Zn/Al-3-600; (d) Zn/Al-3-700; (e) Zn/Al-3-800; (f) S-700 and (g) S-800.

could be influenced by the presence of the parent Zn/Al-2 hydrotalcite because the amount of ZnO formed at 500 °C was still very low. On the contrary, for sample Zn/Al-3-500, with a higher Zn content, the amount of ZnO formed at 500 °C was enough to produce the ZnO typical reflectance spectrum. It is worth noting that both uncalcined hydrotalcite samples, Zn/Al-2 and Zn/Al-3, show DRS spectra (not shown for the sake of brevity) where the reflectance increases from 80% to 100% starting from ca. 375 nm. This wavelength value corresponds to the inflection point in the spectrum of Zn/Al-2-500 reported in Fig. 6(a).

ZnO is an indirect semiconductor [24] and the band gap energies of the samples, estimated from the tangent lines in the plots of the modified Kubelka–Munk function, $[F(R'_\infty)h\nu]^{1/2}$ vs. the energy of exciting light [25], give rise to band-gap values ranging between 3.20 and 3.65 eV, as reported in Table 1. The band gap values decrease by increasing the calcination temperature indicating that the ZnO crystalline phase was predominant on respect to the spinel one, both for Zn/Al-2 and Zn/Al-3 samples. From element chemical analysis data and bearing in mind that in the well crystallized samples (i.e., those calcined at high temperature) Zn is present as ZnO and as the spinel, while the only Al-containing phase is the spinel, we can conclude that sample Zn/Al-2-700 contains 57% ZnO and 43% spinel (mass percentage), while for sample Zn/Al-3-800 these values were 67 and 33%, respectively.

The inset in Fig. 6 shows the DRS spectra for samples S-700 and S-800. Sample S-700 shows the typical broad band spectrum, indicating the presence of a small amount of ZnO. However the spectrum for sample S-800 is dramatically different and the features can be attributed to those ascribed to the pure spinel structure, in agreement with the chemical analyses and literature [26].

3.2. Photoreactivity experiments

Blank reactivity experiments were performed under the same experimental conditions used for the photo-reactivity runs but in the absence of catalyst, oxygen or light. No reactivity was observed in all these cases so that it was concluded that the simultaneous presence of O_2, catalyst, and irradiation was needed for degradation of 2-propanol. The solid samples showed strong adsorption of the substrate under dark conditions. The photore-

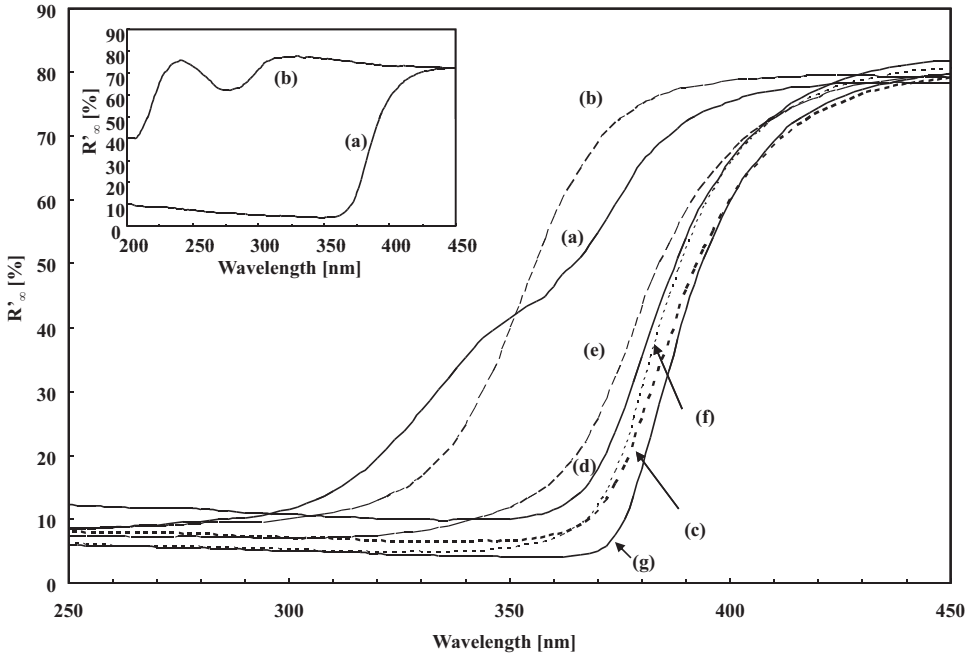

Fig. 6. Diffuse reflectance spectra of: (a) Zn/Al-2-500; (b) Zn/Al-2-600; (c) Zn/Al-2-700; (d) Zn/Al-3-500; (e) Zn/Al-3-600; (f) Zn/Al-3-700 and (g) Zn/Al-3-800. Inset: (a) S-700 and (b) S-800.

activity runs started after the system achieved the steady state conditions in the darkness, i.e., when the concentration of 2-propanol remained constant with time (ca. 1 h was necessary). Fig. 7 reports the values of 2-propanol concentration vs. irradiation time for runs carried out in the presence of calcined Zn/Al-2 and Zn/Al-3 samples. As above mentioned, a strong adsorption of the substrate was observed because the concentration of 2-propanol in the gas phase at steady state conditions resulted ca. 10–20% of the initial one (see Fig. 7). Concerning Zn/Al-2 and Zn/Al-3 powders calcined at 500 °C (Fig. 7(a) and (d)), a moderate photo/thermodesorption was observed during the first stages of the photocatalytic run. 2-Propanol slow desorption throughout all

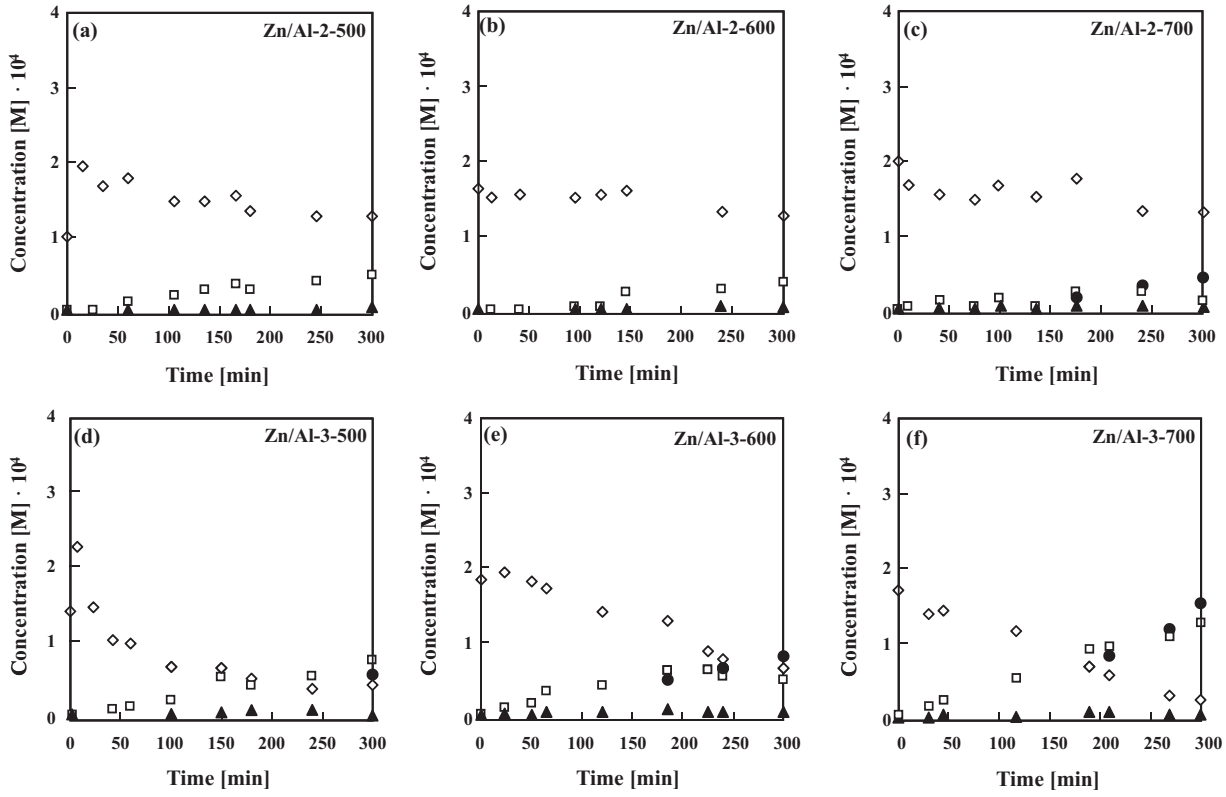

Fig. 7. Evolution of 2-propanol (◊), propanone (□), acetaldehyde (▲) and CO_2 (●) concentrations vs. irradiation time in the gas–solid system in the presence of (a) Zn/Al-2-500; (b) Zn/Al-2-600; (c) Zn/Al-2-700; (d) Zn/Al-3-500; (e) Zn/Al-3-600 and (f) Zn/Al-3-700.

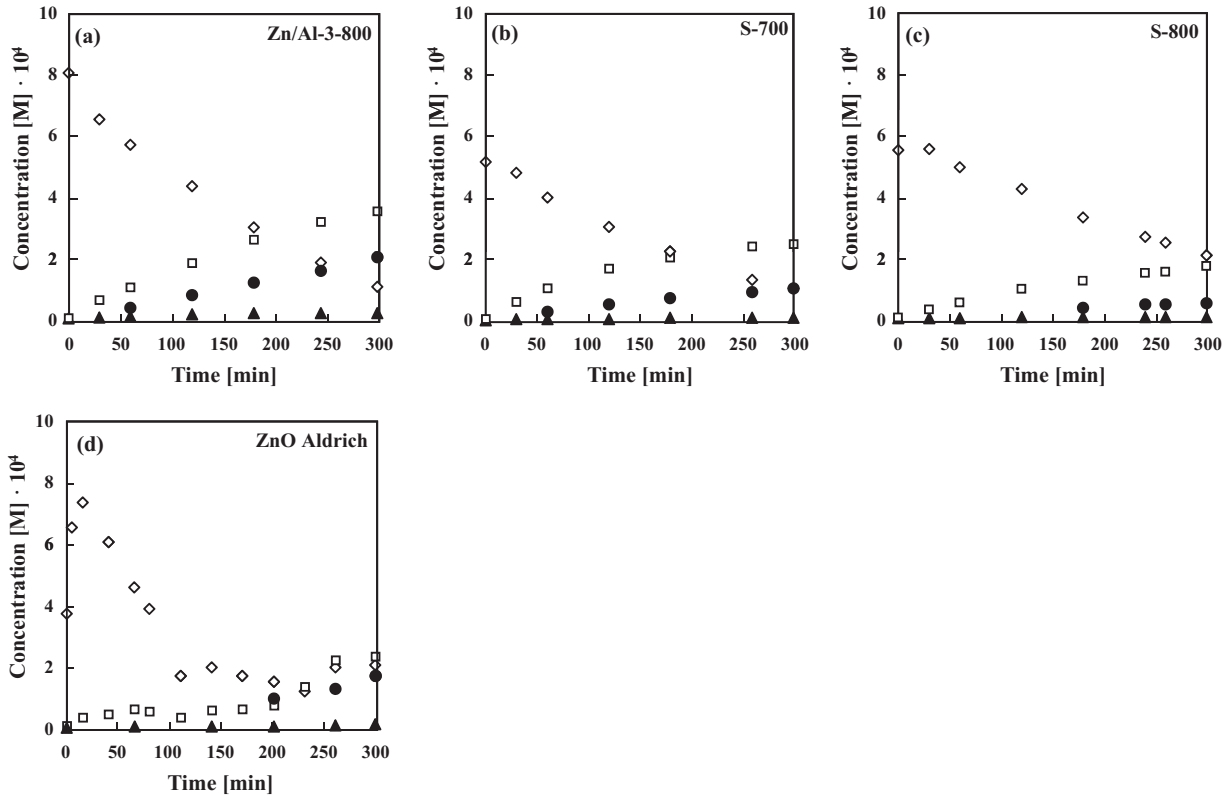

Fig. 8. Evolution of 2-propanol (◊), propanone (□), acetaldehyde (▲) and CO_2 (●) concentrations vs. irradiation time in the gas–solid system in the presence of (a) Zn/Al-3-800; (b) S-700; (c) S-800 and (d) ZnO Aldrich.

the runs probably occurred simultaneously to the photo-oxidation reaction. A decrease of 2-propanol concentration is clearly evident only in Fig. 7(f). In any case, 2-propanol was adsorbed and then desorbed during the photocatalytic runs, although it is possible to establish that its photo-oxidation actually occurred, as propanone and acetaldehyde were found [17]. Carbon dioxide was also detected in the runs carried out by using all the three calcined Zn/Al-3 samples, whereas total oxidation of 2-propanol to CO_2 and H_2O occurred only in the presence of Zn-Al-2-700.

The perusal of Fig. 7 reveals that both parameters, calcination temperature (as reported also for TiO_2 prepared in sophisticated way [27]) and Zn content, strongly influenced the photo-catalytic behaviour. As far as Zn/Al-3 samples are concerned, the total oxidation of 2-propanol, for instance, slightly increased by increasing the calcination temperature. This increase of activity can be attributed to the increasing amount of ZnO in the sample. Table 1 reports the amount of CO_2 obtained after 5 h of photocatalytic reaction that accounts for the activity of the powder under investigation. It is possible to establish, as a general trend, that the photocatalytic activity increased by increasing the calcination temperature and by increasing the Zn content in the powders; indeed, Zn/Al-3-700 was the most photoactive sample (see Fig. 7). In order to ascertain this trend a Zn/Al-3 sample calcined at 800 °C was prepared. Fig. 8(a) reports the evolution of 2-propanol, intermediates and CO_2 during the photocatalytic run and it is evident that this sample showed to be more photo-active than the Zn/Al-3-700 one. It is worth noting that no strong adsorption of 2-propanol, observed in the previous Zn/Al-3 samples, occurred. Actually the initial concentration of the substrate almost coincides with the nominal initial amount (Fig. 8(a)).

This behaviour could be attributed to different morphological and physico-chemical properties of the Zn/Al-3-800 sample in respect to the Zn/Al-3-500, Zn/Al-3-600, Zn/Al-3-700 samples. SEM observations indicate a platelet-like morphology for the samples calcined up to 700 °C, whereas the sample calcined at 800 °C shows a collapse of this feature with formation of rounded edges particles. The almost spherical shape of the particles along with their very low specific surface area could be responsible for the less significant adsorption of 2-propanol.

The photocatalytic reaction by using Zn/Al-3-800 proceeded also with formation of propanone, acetaldehyde and carbon dioxide. The amount of CO_2 obtained by using this sample, reported in Table 1, was the maximum among the Zn/Al samples, indicating that the increase of the calcination temperature and Zn content had a positive effect on the activity of the powder.

Fig. 8 also reports the photocatalytic activity of samples S-700 and S-800 (obtained after samples Zn/Al-3-700 and 800 were submitted to a treatment with NaOH in order to eliminate ZnO).

2-Propanol adsorption in dark conditions (see Figs. 7(f) and 8) was lower for S-700 than for the untreated powder Zn/Al-3-700. This lower adsorption ability can be explained by considering the collapse of the platelet like structure (Fig. 5), due to the NaOH treatment that, as reported above, seems to favour 2-propanol adsorption. On the contrary, S-800 sample showed a higher adsorption ability than sample Zn/Al-3-800, probably due to the presence of porosity (Fig. 3) related to the absence of a platelet like structure and a higher SSA (Table 1).

As far as the photoactivity of S-700 and S-800 is concerned, the reactivity seems to decrease with the calcination temperature (less propanone and CO_2 were formed) but this behaviour is due to the fact that S-800 consists only of spinel (less active than ZnO) while S-700 still contains ZnO.

For the sake of comparison with the home prepared samples, a run was carried out with bare commercial ZnO (Aldrich). The initial concentration of substrate in the gas phase resulted lower than 8.7×10^{-4} M, due to the adsoption of 2-propanol onto the surface

of the photocatalyst under dark conditions, whereas an initial photodesorption of 2-propanol was observed during the photocatalytic reaction, and propanone, traces of acetaldehyde and CO_2 were found. A perusal of Table 1 indicates that 2-propanol was photooxidized more efficiently in the presence of Zn/Al-3-800; indeed, a more significant amount of CO_2 was produced in the presence of the latter sample than in the presence of commercial ZnO.

4. Conclusions

Two series of Zn,Al–CO_3 layered double hydroxides (LDH) with different Zn^{2+}/Al^{3+} molar ratios have been prepared and used as precursors to obtain composites containing ZnO and $ZnAl_2O_4$. By varying both the Zn^{2+}/Al^{3+} molar ratio during the preparation of the LDH precursor and the calcination temperature (500–800 °C) of the LDH solids with different characteristics were obtained.

For both Zn^{2+}/Al^{3+} molar ratios, solids already from 500 °C ZnO and $ZnAl_2O_4$ were formed and the crystallinity of these two phases increased by increasing the calcination temperature.

A pure spinel phase was obtained upon a basic post-treatment in NaOH solution of the samples calcined at 800 °C. All the samples were tested for the photodegradation of 2-propanol in gas–solid regime and all of them resulted active as heterogeneous photocatalysts. Propanone was obtained as a major intermediate product whereas acetaldehyde was also identified. CO_2, as the final oxidation product, appeared only when Zn/Al-2-700 and calcined Zn/Al-3 samples were used. The photocatalytic activity of the samples, evaluated by the amount of CO_2 produced, increased by increasing the Zn^{2+}/Al^{3+} molar ratio and the calcination temperature of the solids. This finding can be attributed to the increase of the ZnO amount and of the crystallinity of the solids. Zn/Al-3-800 was the most photoactive sample and showed to be more photoactive also than a commercial ZnO sample. After treatment of some selected samples with NaOH to partially or completely remove ZnO, the photocatalytic activity decreased, indicating that the ZnO phase was more active than the $ZnAl_2O_4$ spinel one.

Acknowledgements

G.M., E.G.L. and L.P. wish to thank MIUR and INCA for financial support. D.C., M.A., C.M., and V.R. acknowledge financial support from MEC (Grant MAT2009-08526).

References

[1] M. Addamo, V. Augugliaro, A. Di Paola, E. García-López, V. Loddo, G. Marcì, R. Molinari, L. Palmisano, M. Schiavello, J. Phys. Chem. B 108 (2004) 3303–3310.
[2] S. Liu, J. Yu, M. Jaroniec, J. Am. Chem. Soc. 132 (2010) 11914–11916.
[3] (a) G. Marcì, V. Augugliaro, M.J. López-Muñoz, C. Martín, L. Palmisano, V. Rives, M. Schiavello, R.J.D. Tilley, A.M. Venezia, J. Phys. Chem. B 105 (2001) 1026–1032;
(b) G. Marcì, V. Augugliaro, M.J. López-Muñoz, C. Martín, L. Palmisano, V. Rives, M. Schiavello, R.J.D. Tilley, A.M. Venezia, J. Phys. Chem. B 105 (2001) 1033–1040.
[4] J. Yu, X. Yu, Environ. Sci. Technol. 42 (2008) 4902–4907.
[5] S.K. Kansal, M. Singh, D. Sud, J. Hazard. Mater. 141 (2007) 581–590.
[6] R. Comparelli, E. Fanizza, M.L. Curri, P.D. Cozzoli, G. Mascolo, A. Agostiano, Appl. Catal. B 60 (2005) 1–11.
[7] (a) S. Brosillon, L. Lhomme, C. Vallet, A. Bouzaza, D. Wolbert, Appl. Catal. B 78 (2008) 232–241;
(b) V. Augugliaro, S. Coluccia, E. García-López, V. Loddo, G. Marcì, G. Martra, L. Palmisano, M. Schiavello, J. Catal. 235 (2005) 209–220.
[8] S.K. Sampath, J.F. Cordaro, J. Am. Ceram. Soc. 81 (1998) 649–654.
[9] L. Zou, F. Li, X. Xiang, D.G. Evans, X. Duan, Chem. Mater. 18 (2006) 5852–5859.
[10] C.J. Brinker, G.W. Scherer, Sol–Gel Science, Academic Press, Boston, 1990.
[11] F. Cavani, F. Trifiró, A. Vaccari, Catal. Today 11 (1991) 173–301.
[12] V. Rives (Ed.), Study of Layered Double Hydroxides: Present and Future, Nova Sci. Pub., New York, 2001.
[13] D. Carriazo, M. Del Arco, C. Martín, V. Rives, Appl. Clay Sci. 37 (2007) 231–239.
[14] W.T. Reichle, Solid State Ionics 22 (1986) 135–141.
[15] C. Qi, J.C. Amphlett, B.A. Peppley, Appl. Catal. A 302 (2006) 237–243.
[16] F. Li, J. Liu, D.G. Evans, X. Duan, Chem. Mater. 16 (2004) 1597–1602.
[17] G. Marcì, E. García-López, L. Palmisano, D. Carriazo, C. Martín, V. Rives, Appl. Catal. B 90 (2009) 497–506.
[18] C. Busetto, G. Del Piero, G. Manara, F. Trifiró, A. Vaccari, J. Catal. 85 (1984) 260–266.
[19] G.W. Brindley, S. Kikkawa, Am. Miner. 64 (1979) 836–843.
[20] E.M. Seftel, E. Popovici, M. Mertens, K. Witte, G. Tendeloo, P. Cool, E.F. Vansant, Micropor. Mesopor. Mater. 113 (2008) 296–304.
[21] A. Patzkó, R. Kun, V. Hornok, I. Dekany, T. Engelhardt, N. Schall, Colloid Surf. A: Physicochem. Eng. Aspects 265 (2005) 64–72.
[22] X. Zhao, F. Zhang, S. Xu, D.G. Evans, X. Duan, Chem. Mater. 22 (2010) 3933–3942.
[23] K.S.W. Sing, D.H. Everett, R.A.W. Haul, L. Moscou, R. Pierotti, J. Rouquerol, T. Sieminiewska, Pure Appl. Chem. 57 (1985) 603–620.
[24] C. Wang, Q. Li, B. Mao, E. Wang, C. Tian, Mater. Lett. 62 (2008) 1339–1341.
[25] J. Torrent, V. Barrón, Encyclopedia of Surface and Colloidal Science, Marcel Decker Inc., New York, 2002.
[26] S.F. Wang, F. Gu, M.K. Lü, X.F. Cheng, W.G. Zou, G.J. Zhou, S.M. Wang, Y.Y. Zhou, J. Alloy Compd. 394 (2005) 255–258.
[27] J. Yu, B. Wang, Appl. Catal. B 94 (2010) 295–302.